Desalination and Water Treatment
www.deswater.com

doi: 10.1080/19443994.2015.1101716

57 (2016) 19677–19689
September

Taylor & Francis
Taylor & Francis Group

Physical surface modification of nanoporous TFC membranes using UV irradiation for water desalting; determination of best conditions

H. Soltani Afarani, Y. Mansourpanah*

Membrane Research Laboratory, Lorestan University, P.O. Box 68137-17133, Khorramabad, Iran, Tel. +98 6633120611; Fax: +98 6633120612; emails: mansourpanah.y@lu.ac.ir, mansourpanah.y@gmail.com (Y. Mansourpanah)

Received 23 February 2015; Accepted 25 September 2015

ABSTRACT

The main goal of this study was to determine the desirable conditions to modify the surface properties of poly(piperazineamide) thin-layer membranes using UV irradiation without using any chemical reagents. The obtained membranes were exposed to UV irradiation under different conditions such as irradiation time (30, 60, and 120 s) and its power (125 and 250 w) as well as irradiation distance (5, 10, and 15 cm) between the UV lamp and the thin layers. SEM, AFM, ATR-IR, water contact angle, and nanofiltration setup were utilized to determine the properties of the obtained thin layers. SEM images clearly illustrated the alterations in the surface morphology. Reduction in pore sizes of the thin layers was proven by AFM results under different conditions. The rejection capability of the unmodified thin layer against NaCl and Na_2SO_4 was 12 and 60%, respectively; which was increased to about 42 and 82%. Flux recovery ratio test showed the ability of the modified thin layers to prevent the settlement of foulants. The results showed that irradiation time was more important than irradiation distance and irradiation power.

Keywords: Surface modification; Thin film; UV irradiation; Performance; Fouling

1. Introduction

Since energy is too expensive, the use of membrane technology in separation applications plays an important role in reducing the environmental impacts and costs of industrial processes. The membrane process has been used in many applications such as wastewater treatment, industrial water production, water softening, and the separation of compounds having different molecular weights. Most commercial membranes have a thin-film composite (TFC) structure which presents key advantages compared to asymmetric membranes [1,2]. In a TFC membrane, the support layer provides appropriate mechanical strength with low resistance to permeate flux and each layer can be optimized for the desired combination of permeate flux and solute rejection. Several processes have been reported for the preparation of composite NF membranes and interfacial polymerization which was first introduced by Morgan in 1965 [3–6].

A composite membrane is obtained by forming an ultra-thin dense layer on a porous support. Controlling the structure and surface properties of the thin layers are vital for the membrane performance. The composition and morphology of composite membranes prepared by interfacial polymerization depend on various parameters such as thin-layer preparation conditions and post-treatment [2]. The most active

*Corresponding author.

TFC membrane prepared so far is polyamide (PA) [7,8], which employs amine and acid chloride compounds as monomers in interfacial polymerization. The separation performances of the TFC membranes are highly dependent on the conditions used in the interfacial polymerization such as humidity, ambient temperature, and experimental conditions of the reaction [1,3].

Several surface modification techniques have been developed over the recent years (chemical [9], plasma irradiation [10], or UV photo-grafting [11–17]). UV light can be used for surface modification of TFC membranes and has been intensively explored for the controlled functionalization of polymeric membranes [18]. It is well known that photo-induced polymerization is a desirable method for surface modification of polymers. Photo-induction can be used due to its relative simplicity, energy-efficiency, and cost-effectiveness, also photo-induced polymerization is well suited for integration with other technologies to produce desired chemical changes in well-defined two-dimensional regions on a surface.

Absorption of high-energy radiations by polymers induces excitation and ionization and these excited and ionized species become the initial chemical reactants for a series of complicated reactions to release free radicals that may induce the polymerization of the monomers. The polymer to be surface modified is usually immersed in a monomer solution, so that the radicals produced on the polymer surface can immediately initiate the copolymerization of the monomer. In addition to producing free radicals, exposure of polymers to radiations can lead to other extensive chemical reactions and physical changes which may have both detrimental and beneficial consequences in determining the end uses of the polymers. The main chemical reactions are radical producing, chain scission reactions, cross linking reactions, formation of peroxide groups, decomposition of peroxide groups producing radicals, and graft copolymerization. In the whole chemical reaction, the beneficial consequences included the production of cross-linking, grafting on the surface of the polymers, and copolymerization and the detrimental consequences included inducement of chain scission reactions (bond breaking) [19]. While a moderate number of cross-linkers improve the physical properties of the polymers, chain scission reactions are usually detrimental and result in soft and weak materials. However, in many cases, cross-linking and chain scission reactions occur simultaneously. Chemical nature and morphology of the material can determine the predominance of these two reactions [20–22].

Comprehensive literature review showed several works that had used UV irradiation accompanied by chemical regents [23–27]. In this study, a few thin-film composite nanofilteration membranes [poly(piperazineamide) thin layer] were fabricated and modified with UV irradiation without using any chemical regents. For this purpose, the obtained thin layers were exposed to UV irradiation under different times, powers, and distances. UV irradiations were used instantaneously with interfacial polymerization reaction. Our study focused on changing and modifying the thin-layer characteristics without using any chemical reagents to determine optimal conditions. The relationship between the membrane characteristics and different time/power/distance of UV irradiation was investigated. The rejection capability and separation performance of the flat-sheet composite NF membranes were measured using NaCl and Na_2SO_4 as feed solutions. The membrane fouling resistance was studied using Bovine Serum Albumin (BSA) solution. The structure and chemical composition of the obtained TFC nanofiltration membranes were investigated using SEM, AFM, water contact angle, and ATR-IR techniques.

2. Experimental

2.1. Materials and apparatus

Polyethersulfone (PES Ultrason E6020P with MW = 58,000 g/mol) was obtained from BASF Company (Germany). Polyvinylpyrrolidone (PVP, 25,000 g/mol), dimethylformamide (DMF), piperazine (PIP), and polyethylene glycol 600 (PEG-600) from Merck were used. Na_2SO_4 and NaCl salts (Merck) were chosen to investigate the rejection capabilities of the membranes. BSA powder [some properties are as follows: assay > 96%, mol wt.; 66 kDa, pH ≈ 7, solubility > 40 mg/mL inH_2O] was obtained from Sigma. Trimesoyl chloride (TMC) was purchased from Fluka. UV apparatus was similar to Ref. [28]. Distilled water was used throughout the study.

2.2. PES support preparation

PES support was prepared by dissolving 18 wt.% PES in DMF with 10 wt.% PVP, 3 wt.% acrylic acid, and 5 wt.% PEG 600 as additives and stirring for 4 h at 50˚C. The stirring was carried out at 300 rpm. After formation of a homogeneous solution, the dope solution was held at the ambient temperature for around 4 h to remove the air bubbles. Afterward, the dope solution was cast on the non-woven polyester (with 150 μm thickness) at 150 μm heights using a film applicator at room temperature and in 37% humidity without evaporation. After coating, the membrane was

immersed into a distilled water bath for at least 24 h to ensure complete phase separation.

2.3. Fabrication of thin-film composite membranes

The PES support membrane was clamped between two Teflon (height: 0.7 cm, inner cavity: 7.5 × 20 cm^2). An aqueous phase containing PIP (0.15 wt.%) and TEA (0.4 wt.%) was poured on the top of the support membrane and was allowed to get wet for 10 min at the ambient temperature. The surface was rolled by a soft roller to eliminate any little air bubbles during the wetting procedure. After draining off the excess solution, the organic solution (n-hexane) of TMC (0.1 wt.%) was poured into the frame where the conventional interfacial polymerization reaction took place. The membrane was immediately exposed to UV irradiation and the reaction was carried out between TMC and PIP. The schematic of the process is shown in Fig. 1. After 10 min excess organic solution was removed and the membrane was exposed to 70°C hot air for 5 min. To form a poly(piperazineamide) skin layer, the dipping process was carried out in such a way that only the external surface was coated with the reactants.

The concentration of TMC and PIP and their proportions (2(TMC)/3(PIP)) were selected according to the available literature [29]. Table 1 shows the conditions of the fabrication of the thin-layer membranes. TEA was used as a base to progress the interfacial polymerization reaction to form the polyamide layer.

2.4. Characterization of membranes

The surface and the cross section of the membranes were examined by using a Philips Scanning Electron Microscope model X130 (SEM). The membrane samples were frozen in liquid nitrogen and

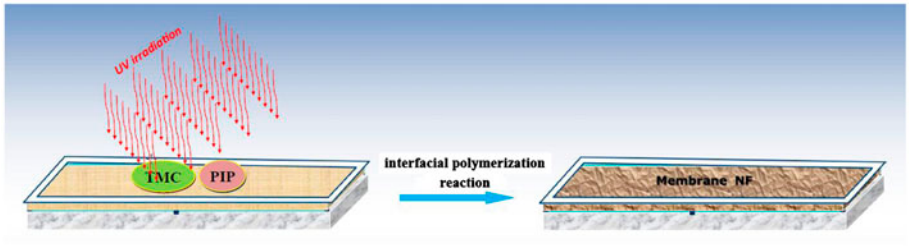

Fig. 1. The schematic illustration of UV irradiation.

Table 1
Conditions of the thin-layer fabrication

Name	Power (W)	Distance (cm)	Time (s)
E_0	–	–	–
E_1	250	15	30
E_2	250	15	60
E_3	250	15	120
E_4	250	10	30
E_5	250	10	60
E_6	250	10	120
E_7	250	5	30
E_8	250	5	60
E_9	250	5	120
E_{10}	125	15	30
E_{11}	125	15	60
E_{12}	125	15	120
E_{13}	125	10	30
E_{14}	125	10	60
E_{15}	125	10	120
E_{16}	125	5	30
E_{17}	125	5	60
E_{18}	125	5	120

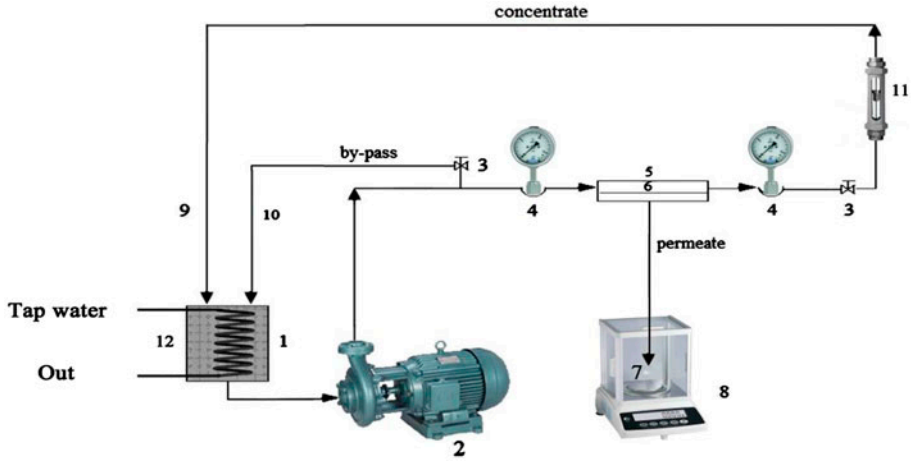

Fig. 2. Cross-flow filtration system.
Notes: (1) feed tank; (2) pumb, (3) value, (4) pressure guage, (5) cassflow cell, (6) membrane, (7) permeate, (8) balance, (9) concentrate, (10) by-pass, (11) flow meter, (12) cooling system.

Table 2
Contact angle measurements with different irradiation times

Membrane	Contact angle (°)
E_0	53 (±1.00)
E_9	49 (±0.81)

were fractured to the pieces with 1-cm^2 surface area. Afterward, they were sputtered with gold and viewed at 25 kV.

Chemical alteration of the membranes was investigated using an Equniox 55 Bruker FT-IR spectrometer (purchased from Germany) equipped with an attenuated total reflection (ATR) attachment.

Atomic force microscopy (AFM, non-contact mode) was used to analyze the surface morphology and roughness of the membranes. The AFM apparatus was a DualScope™ scanning probe-optical microscope (DME model C-21, Denmark). Small square pieces of the prepared membranes (approximately 1 cm^2) were cut and glued on a glass substrate. The membrane surfaces were analyzed in a scan size of 1 × 1 μm.

The contact angle is the angle at which a liquid interface meets a membrane surface. The contact angle results from the surface free energies between the liquid and membrane. The contact angle is commonly used in membrane material science to describe the relative hydrophobicity/hydrophilicity of a membrane surface [30]. The static contact angles were measured with a contact angle measuring instrument (G10, KRUSS, Germany). Deionized water was used as probe liquid in all measurements and the contact angles between water and the membrane surface were measured for the evaluation of the membrane hydrophilicity. To minimize the experimental error, the contact angles were measured at five random locations for each sample and their average value was reported.

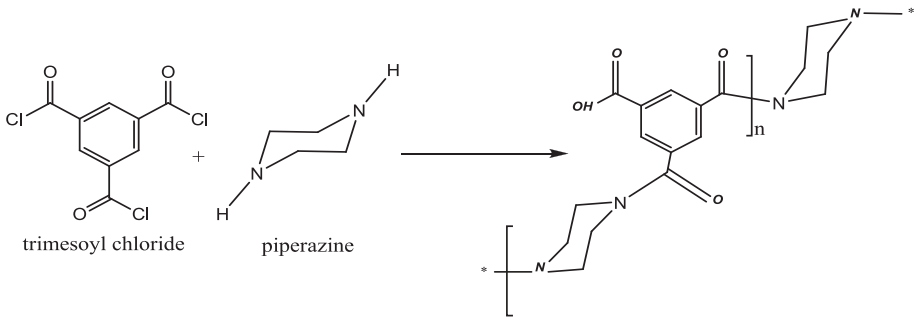

Fig. 3. The mechanism of interfacial polymerization.

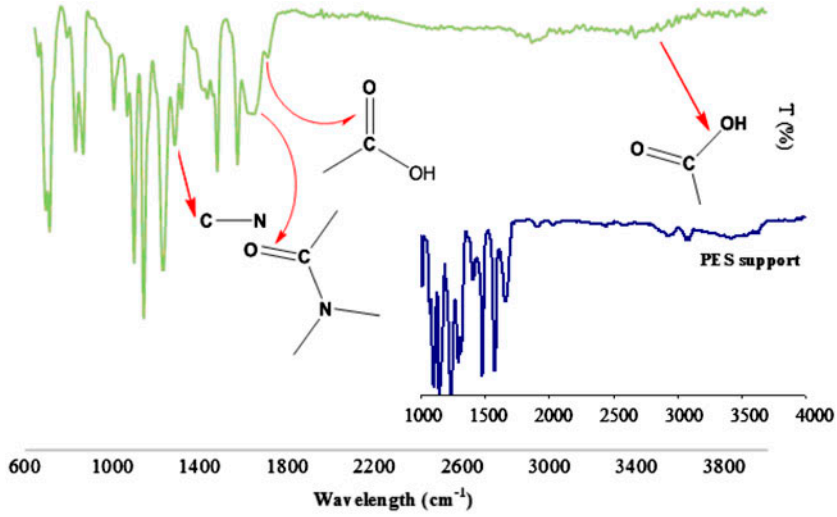

Fig. 4. FTIR/ATR spectra of the PA membrane surface.

2.5. Membrane performance evaluation

The performances of the prepared membranes were analyzed by applying a batch cross flow system (Fig. 2). The membrane surface area in the filtration cell was 22 cm^2. The flux of each membrane was determined at 10 min intervals under 0.8 MPa transmembrane pressures. The experiments were carried out at 25°C. The cross-flow velocity was approximately 0.6 m/s for all tests. Test results are displayed in Table 2.

Permeation rate and salt rejection were determined for all membranes using different ionic solutions (NaCl, Na_2SO_4) of 1,000 ppm concentration. The rejection values were calculated using the following equation:

$$R\,\% = \left[1 - \frac{\lambda_p}{\lambda_f}\right] \times 100 \quad (1)$$

where λ_p and λ_f are ion conductivities in permeate and feed, respectively [31]. The ion rejection was investigated by measuring the permeate conductivity using a conductivity meter (Hanna 8733 Model, Italy).

2.6. Antifouling properties and flux recovery

Fouling can be quantified by the resistance appearing during the filtration and cleaning can be specified by the removal of this resistance. The resistance occurs due to the formation of a cake or gel layer on the membrane surface. The flux (J) through the cake and the membrane may be described by the following equation:

$$J = \frac{m}{A\Delta t} \quad (2)$$

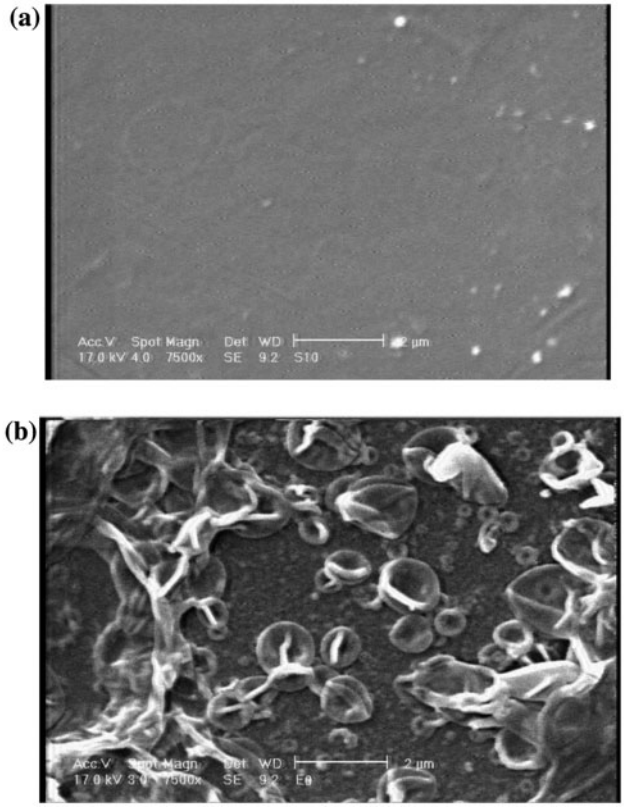

Fig. 5. SEM images of the surfaces of: (a) PES support and (b) non-irradiated PIP-TMC thin layer.

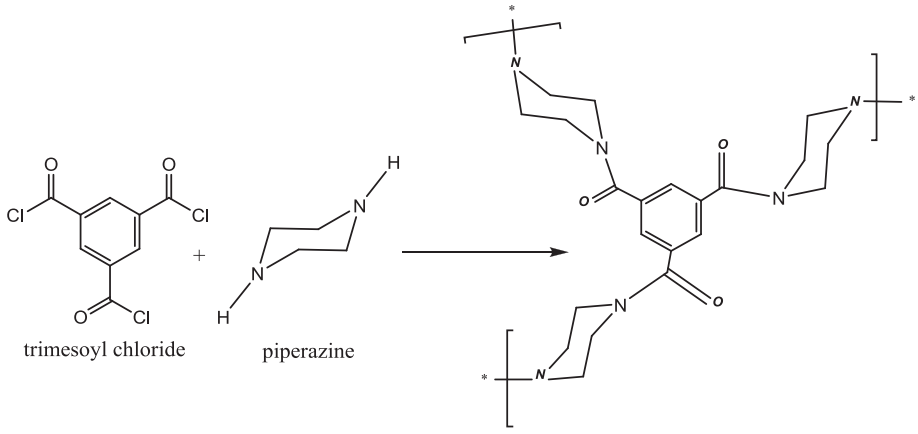

Fig. 6. Polymerization process in 3D.

where m is the mass of the permeated water, A is the membrane area, and Δt is the permeation time.

After water flux measurement (J_{wi}), the solution reservoir was refilled with a 0.1-g/L BSA solution, and the flux was measured (J_p). After 2 h of filtration, the membrane was washed with deionized water for 10 min and the water flux of the cleaned membranes was measured (J_{wc}). In order to evaluate the fouling resistance capability of the membrane, the flux recovery ratio (FRR) was calculated using the following equation:

$$\mathrm{FRR} = \left(\frac{J_{wc}}{J_{wi}}\right) \times 100 \tag{3}$$

R_r and R_{ir} which are described by Eqs. (4) and (5) show reversible deposition and irreversible fouling, respectively [32]:

$$R_r\,(\%) = \left(\frac{J_{wc} - J_p}{J_{wi}}\right) \times 100 \tag{4}$$

$$R_{ir}\,(\%) = \left(\frac{J_{wi} - J_{wc}}{J_{wi}}\right) \times 100 \tag{5}$$

3. Results and discussion

3.1. Mechanism of interfacial polymerization reaction

In this study, TMC and PIP were used as reactants and triethylamine was used as acid acceptor. The interfacial polymerization reaction mechanism is shown in Fig. 3. The terms acyl and aryl halides refer to aliphatic and aromatic derivatives, respectively. They react with water, alcohols, and amines and are widely used in organic synthetic processes whereby the acyl group is incorporated into the target molecules by the substitution of addition–elimination sequence called the acylation reaction.

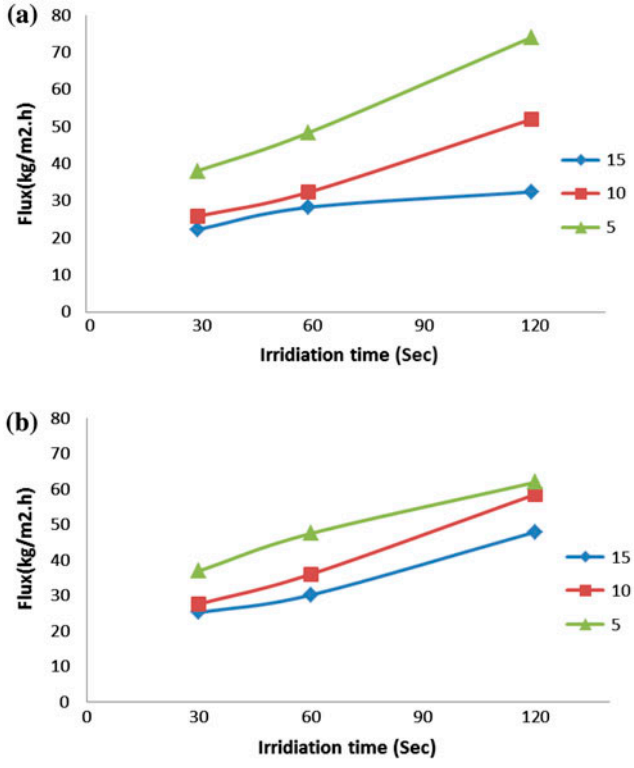

Fig. 7. Effect of irradiation time on the flux and rejection of the thin layer membrane at 250 W.

Table 3
Details of membranes cross-flow filtration for NaCl and Na_2SO_4 salt solution

Name	% *R* Na_2SO_4	% *R* NaCl
E_0	60.42	12.81
E_1	82.20	35.70
E_2	62.41	25.00
E_3	76.02	32.00
E_4	56.52	23.93
E_5	75.56	28.32
E_6	58.41	32.34
E_7	80.47	41.92
E_8	57.45	27.57
E_9	46.38	23.70
E_{10}	72.84	39.05
E_{11}	50.95	17.24
E_{12}	30.56	18.18
E_{13}	75.57	26.40
E_{14}	71.53	26.29
E_{15}	52.68	20.90
E_{16}	80.47	41.92
E_{17}	76.47	27.63
E_{18}	24.64	12.50

The poly(PIP–TMC) chain is expected to contain both cross-linked and non-cross-linked structures containing carboxylic acid groups. The carboxylic acid functional group arises due to the partial hydrolysis of the acyl chloride moiety of TMC. The performance of the poly(piperazineamide) composite membranes is mainly determined by polymerization conditions such as the degree of UV irradiation, monomer types, monomer concentrations, reaction time, curing time, and curing temperature.

3.2. Characterization of the skin layer structure

In order to grasp the chemical structure of the skin layer of the NF membrane, ATR-IR characterization was carried out. The ATR-IR spectrum (Fig. 4), in comparison with the neat PES membrane, indicated that the interfacial polymerization had successfully occurred since a strong band at 1,640 cm^{-1} was present. This is the characteristic of the C=O band of an amide group. The peaks at 1,350 cm^{-1} were assigned to C–N stretching in polyamide. A wide and weak peak at 3,400 cm^{-1} was assigned to some –COOH groups in the obtained skin layer.

In addition, SEM images clearly showed the formation of an established thin layer over the support membrane. Fig. 5(a) belongs to the PES support surface. Based on this image, the membrane support surface presents a smooth and flat surface. On the other hand, Fig. 5(b) which belongs to the thin-layer membrane surface shows a rough and uneven surface due to the formation of a thin layer over the support.

The hydrophilicity of the obtained membranes was evaluated by measuring the static water contact angle. For comparing, Table 2 represents the water contact angles of E_0 and E_9 membranes. The results demonstrated that the hydrophilicity of the thin layers was increased by increasing the UV irradiation time. The contact angle degree of E_0 membrane was 53˚, while the UV-irradiated membrane (E_9) showed lower contact angle, 49˚. The modification of the thin-layer membrane by UV irradiation prominently increased the hydrophilicity of the membranes due to the appearance of –COOH groups on the membrane surface. However, E_9 membrane with a long UV irradiation time exhibited a higher flux and less rejection, that may be attributed to the increase in hydrophilicity as well as destruction of poly(piperazineamide) thin layer.

Although the formation of a skin layer occurs in a short period of time, the UV irradiation might have two secondary effects:

(a) The UV irradiation can break or weaken some bonds (–COCl and N–H) which causes more reactivity. This phenomenon prevents from the hydrolyzation of the remaining –COCl groups to –COOH. Accordingly, some existing undestroyed –COCl groups in the PA chains are used to cross-link when they meet the diffusing diamine, resulting in an increase in 3D growth (Fig. 6) and more densification of the thin film

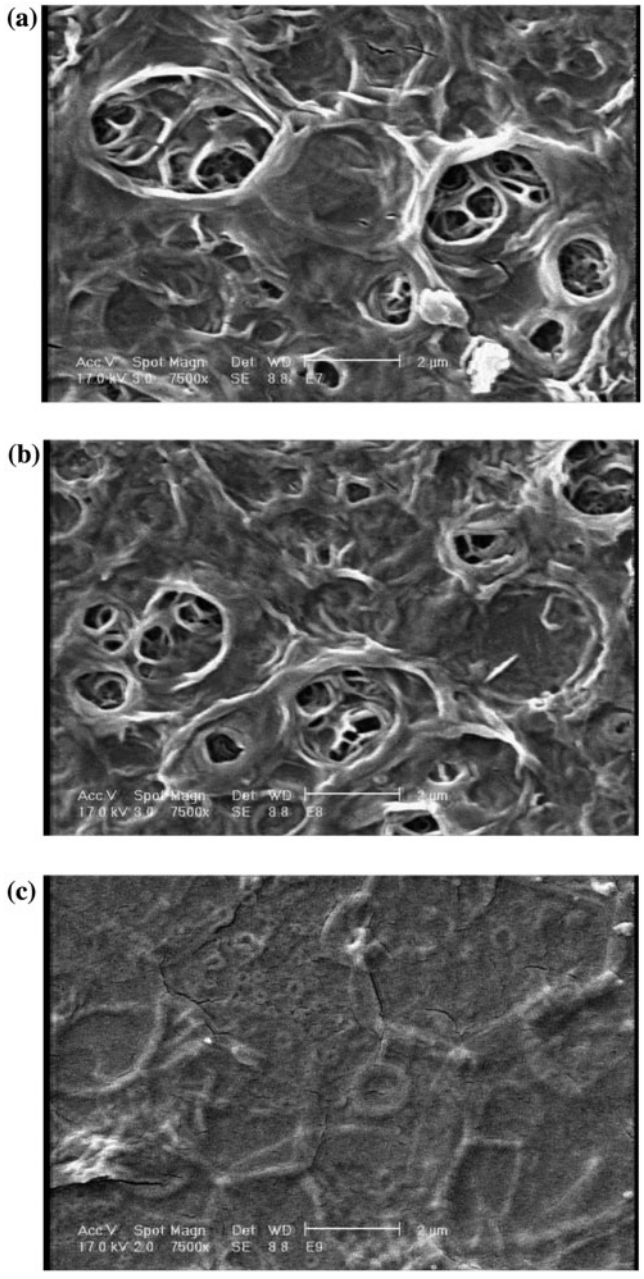

Fig. 8. SEM images of the surfaces of thin-layer membranes: (a) E_7, (b) E_8 and (c) E_9.

[33]. Obviously, this phenomenon declines the flux and increases the rejection capability. (b) The UV irradiation has a wavelength degradation effect on the bonds. This phenomenon affects support membrane (PES) and poly piperazineamide bonds, resulting in higher flux and lower rejection. Details are fully discussed in literature [34]. In fact, the UV irradiation of poly(ethersulfone) membrane involves two parallel compensating processes, cross-linking, and chain scission that determines final membrane transport properties [35]. As will be described in the next sections, in some situations chain scission is predominant and in some other situations cross-linking overcomes the chain scission.

3.3. Effect of irradiation time

The effect of irradiation time (30, 60, and 120 s) on the membrane performance was investigated. The results clearly indicated that the irradiation time affects the membrane performance. As mentioned previously, more polymerization at the beginning of the irradiation results in the 3D growth of polymerization by inducing the diffusing PIP molecules to replace the –OH group of carboxylic acid. Fig. 6 clearly indicates the anticipated mechanism of polyamide layer formation. 3D growth of polymerization results in the elimination of –COOH groups and formation of –CON groups. Consequently, a dense and compressed thin layer is formed. Therefore, polymerization and its 3D growth were accelerated by expanding the UV irradiation time from 30 to 60 s. However, the opposite phenomenon occurred in longer time of UV irradiation (120 s). In other word different UV irradiation times induced two parallel competing processes, cross-linking, and chain scission.

As can be seen in Fig. 7(a) and (b), the lowest flux was achieved for the membranes with 30 s irradiation time. The water fluxes of the non-irradiated and 30, 60, and 120 s irradiated membranes at 250 W and 5 cm interval were approximately 61, 38, 48, and 74 kg/m^2 h, respectively. The flux of salty solutions showed a similar trend. However, the lowest flux in 15 cm distance was achieved for 30 s-irradiated membranes. The water fluxes of 30, 60, and 120 s-irradiated membranes at 250 W and 15 cm distance were approximately 22, 28, and 32 kg/m^2 h, respectively.

The rejection values of NaCl and Na_2SO_4 solutions were also measured. As can be seen in Table 3, the rejections were reduced by increasing the time of UV irradiation. The same rejection trend was observed for NaCl salt. The rejection capability of the membranes for Na_2SO_4 was higher than that of the membranes for NaCl. The performances of the obtained membranes may be explained on the basis of charge, diffusion coefficient, and the size of ions. Cross-linking or 3D growth of polymerization provides fewer passage routes for water and salt through the membrane leading to lower flux and higher rejection. According to the SEM images, the thin layer was formed from the reaction between PIP and TMC. This reaction was catalyzed by UV irradiation at the shortest times (initial

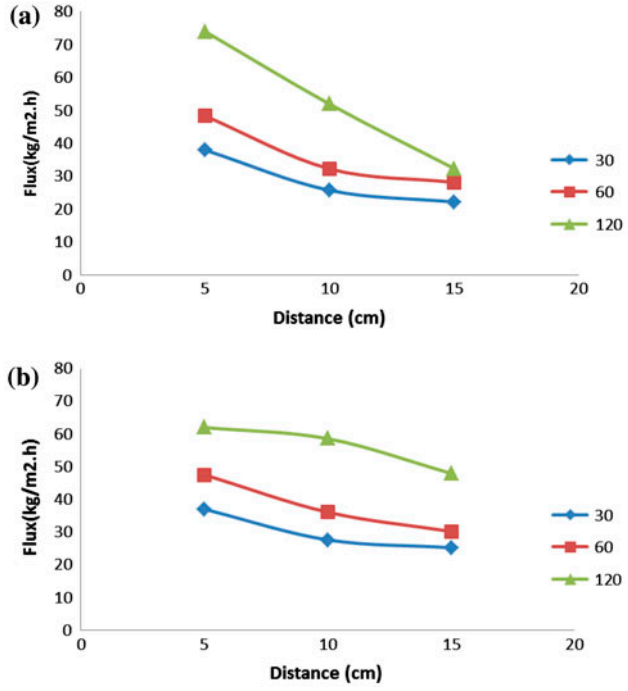

Fig. 9. Effects of UV radiation distance on the flux and rejection of the thin-layer membrane at 125 W.

stages) for the formation of poly(piperazineamide). As can clearly be seen in Fig. 8, the membrane surface structure was changed at longer times of UV irradiation (at next stages) because of the degradation effect of UV irradiation on the bonds and the thin layers (Fig. 5(c)). In fact, SEM images showed that a dense and more compressed thin layer was formed in shorter UV irradiation times. In contrast, some defects were observed due to the damaging of the thin layer at longer UV irradiation time, resulting in higher flux and less rejection.

3.4. Effect of irradiation distance

Generally, UV irradiation is helpful in the formation of thin layers, but not at long times and close distances. In fact, the increase in time and decrease in distance improved the degradation and damaging of the thin layers along with the compressing effect of UV irradiation. In fact, short distances destroyed poly (piperazineamide) thin layer.

Fig. 9 shows the effect of irradiation distance on the performance of the obtained membranes. In lower irradiation powers and longer distances, the flux of the thin-layer membranes was slightly decreased and the rejection was increased (Table 3). The lowest fluxes were recorded for the membranes at the irradiation distance of 15 cm. By increasing the irradiation time, it was clearly seen that the fluxes of most membranes were increased (at distance of 10 and 15 cm). As can be seen in Fig. 9(a), the flux reduction of 60 and 120 s-irradiated membranes was less than that of 30 s. The results obtained from lower power (125 W) irradiation were also reported (Fig. 9(b)).

Fig. 10 belongs to E_1, E_2, and E_3 thin-layer membranes. The comparison of the images indicated that a well established and compressed skin layer was

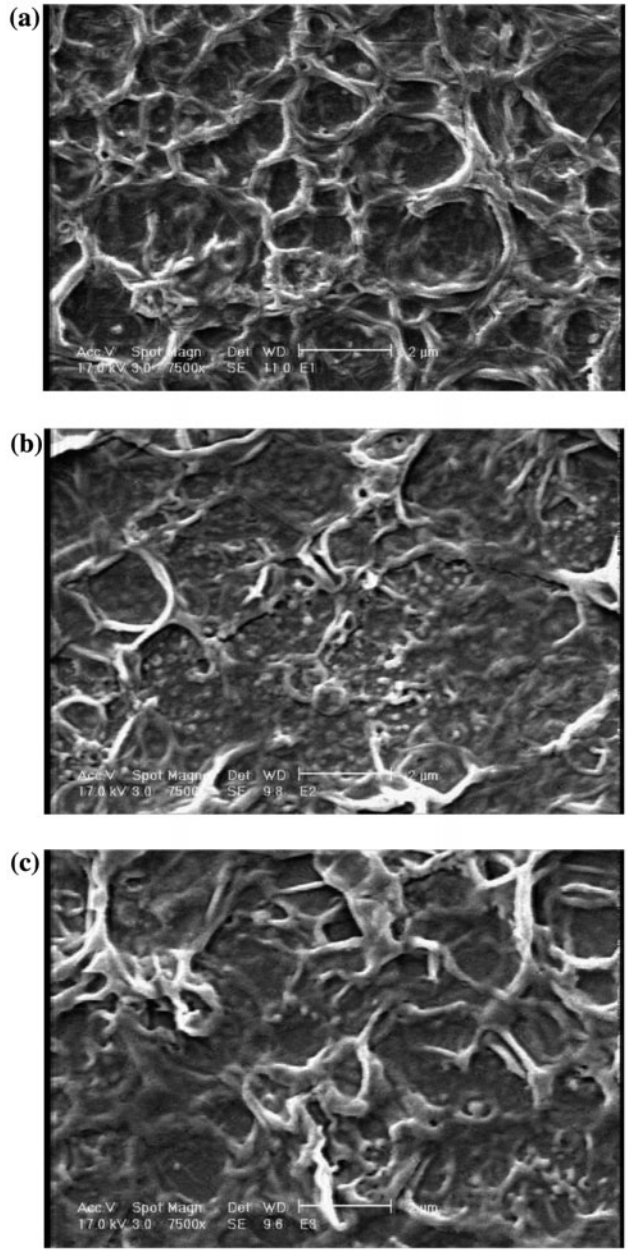

Fig. 10. SEM images of the surfaces of thin layer membranes: (a) E_1, (b) E_2, and (c) E_3.

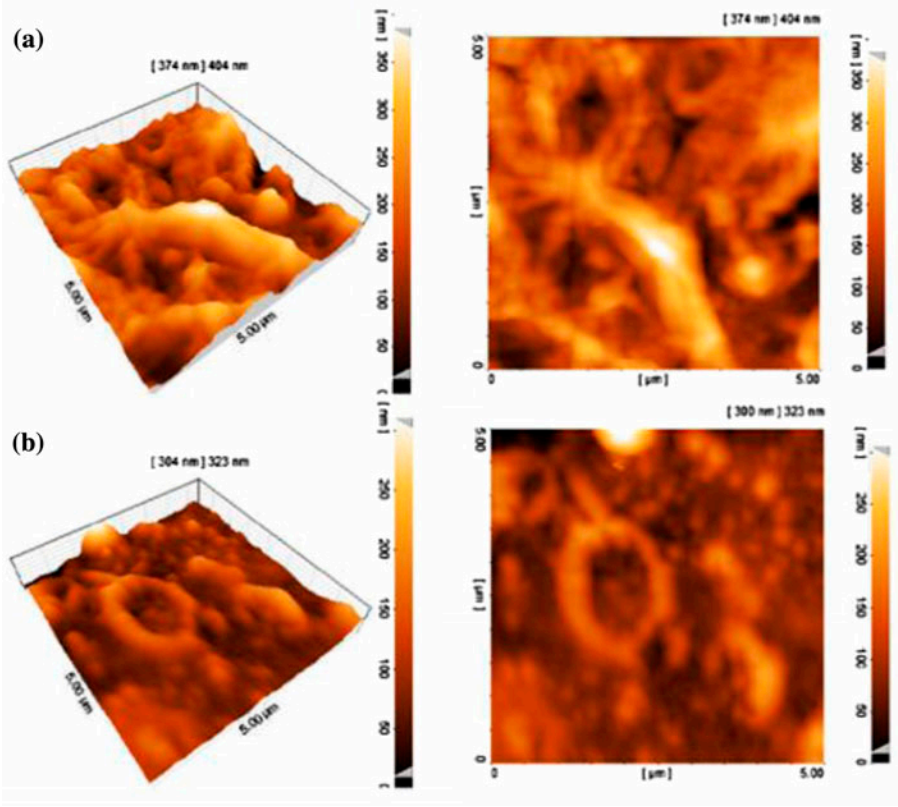

Fig. 11. AFM images of the surfaces of PIP-TMC thin layer membranes: (a) E_{12} and (b) E_{18}.

formed using UV irradiation in longer distances. However, comparing Figs. 10(c) and 8(c) clearly shows that the degradation of the thin layer occurred in shorter distances.

On the other hand, Fig. 11 shows the two- and three-dimensional AFM images of thin layer surfaces. For better comparing, E_{12} and E_{18} with the same irradiation powers and irradiation times were chosen. The main difference of these membranes was the irradiation distance. Based on AFM results, E_{18} thin layer (Fig. 11(b)) showed a dense and compressed thin layer in comparison with E_{12} (Fig. 11(a)). The flatter structure was formed in shorter distance. These AFM images clearly showed the effect of irradiation distance on the morphology of the irradiated thin layers. The surface roughness parameters of the membranes which were explained in terms of the mean roughness (S_a), the root mean square of the Z data (S_q), and the mean difference between the highest peaks and lowest valleys (S_z) were calculated by SPM DME software. The obtained results, which are presented in Table 4, indicated that the roughness parameters of the thin-layer membranes decreased by reducing the irradiation distance. According to the data in Table 4, the values of S_q, S_a, and S_z for E_{12} were 63.7, 63.7, and 332 nm, respectively, which were reduced to 37.1, 28.2, and 202 nm (for E_{18}). However, comparing E_{12} and E_{18} indicated that the roughness parameters were decreased by decreasing the irradiation distance.

Table 4
Surface roughness parameters of different membranes obtained from AFM images

Membrane	Power (w)	Distance (cm)	Time (s)	Roughness parameters (nm)		
				S_q	S_a	S_z
E_{12}	125	15	120	63.7	63.7	332
E_{18}	125	5	120	37.1	28.2	202

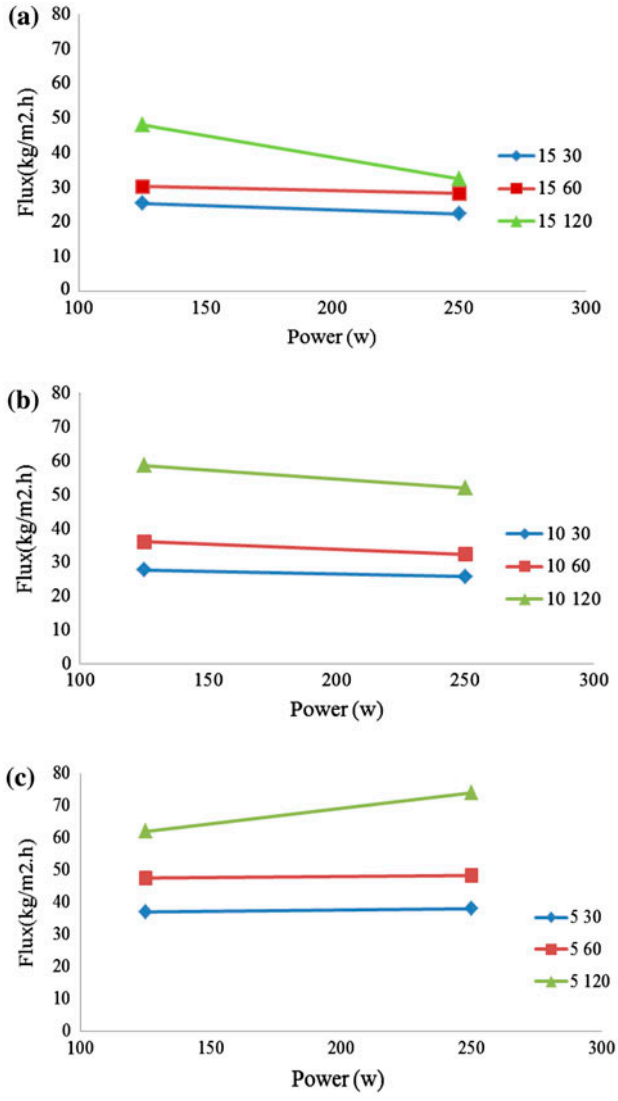

Fig. 12. Effects of UV irradiation power and irradiation times on the flux and rejection of thin layer membranes: (a) 15 cm, (b) 10 cm, and (c) 5 cm.

3.5. Effect of irradiation power

In this work, two different irradiation (source) powers (125 and 250 w) were studied. Lower power of irradiation had a slight effect on the weakening of –COCl and N–H bonds and on degrading of chains. As can be seen in Fig. 12, no significant changes in the flux were observed in two powers except in the longest time of irradiation (120 s).

According to Fig. 12(a) and (b), the fluxes of the thin-layer membranes were decreased by increasing the irradiation power and distance. This may be due to the 3D growing of chains, resulting in the formation of a dense and compressed thin layer. On the other hand, for 5 cm distance, the opposite phenomenon occurred. In fact, by increasing the irradiation power along with decreasing the distance to 5 cm the flux of the thin layer membranes were increased (Fig. 12(c)). As mentioned previously, this may be due to the degradation of thin layer chains. Accordingly, the sensible differences between two powers might be seen at longer distances.

Fig. 13 represents the surface images of poly(piperazineamide) thin layers in the presence of 125 W

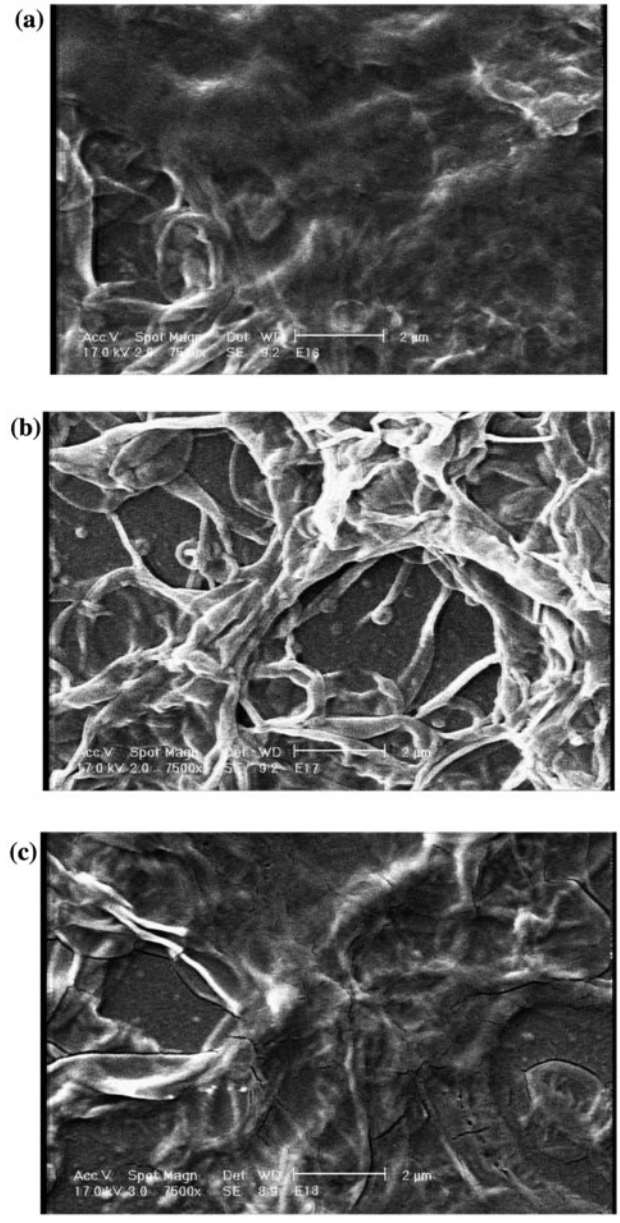

Fig. 13. SEM images of the surfaces of thin-layer membranes: (a) E_{16}, (b) E_{17}, and (c) E_{18}.

Table 5
Performance of thin-layer membranes at presence of UV irradiation

Membrane	R_{ir}	R_r	FRR
E_0	45	22	55
E_7	15	10	85
E_8	24	12	76
E_9	45	20	55
E_{16}	32	30	68
E_{17}	33	32	67
E_{18}	35	40	65

irradiation power and 5 cm distance. Figs. 13(a) and (b) illustrate the well established and compressed thin layers whose morphologies were slightly changed to form a defected structure at 120 s irradiation. As Table 1 shows, the fabrication conditions for E_7, E_8, and E_9 with E_{16}, E_{17}, and E_{18} were the same except in the irradiation powers.

According to the obtained results, we found that the order of the importance of the conditions was as follows: irradiation time > irradiation distance > irradiation power.

3.6. Investigating the fouling properties

As mentioned in performance trials, the feed was a BSA suspension with a superior fouling tendency. Protein molecules can deposit on the surface of the membrane and gradually form a layer on the membrane surface [32]. The flux properties of the membranes were remarkably declined during 2 h of filtration by BSA solution.

The antifouling properties, i.e. FRR, reversible resistances (R_r), and irreversible resistances (R_{ir}) of the irradiated and non-irradiated membranes are summarized in Table 5. The FRR was increased from 55% for non-irradiated membrane (E_0 membrane) to about 85% for E_7 membrane.

We believe that the main factor responsible for the reduction of fouling tendency is increasing the hydrophilicity of the thin layers due to the presence of more –COOH functional groups and UV-irradiation. On the other hand, the creation of cracks and defects on the thin layer surface resulted in lower FRR (see Fig. 8(c) for E_9). The FRR of E_9 membrane was about 55%. However, E_7 membranes showed the least fouling tendency due to the formation of a more establish and uniform surface. On the other hand, E_9 membrane revealed lower FRR in spite of more compressed and flatter surface and higher surface hydrophilicity. E_{16}, E_{17}, and E_{18} membranes with the FRR amounts near 68, 67, and 65% respectively, showed FRR more than E_9 membrane which may be due to the effect of lower irradiation power.

4. Conclusion

According to this study, shorter time of irradiation (about 30 s) caused slightly high rejection and low flux. This was probably due to the increase of polymerization process as well as the formation of a more established poly(piperazineamide) thin layer. However, longer time of irradiation resulted in thin layer degradation and, therefore, declined the rejection value but, at the same time, led to the formation of –COOH functional groups. The formation of further –COOH functional groups decreased the fouling tendency and increased the surface hydrophilicity of the membranes. Finally, it can be concluded that the UV irradiation might be considered as a physical modification procedure and it showed a remarkable and outstanding effect on the modification of the thin layers. In contrast, longer times and shorter distances of UV irradiation showed no significant and desirable effect.

References

[1] Y. Mansourpanah, K. Alizadeh, S.S. Madaeni, A. Rahimpour, H. Soltani Afarani, Using different surfactants for changing the properties of poly(piperazineamide) TFC nanofiltration membranes, Desalination 271 (2011) 169–177.
[2] M.R. Teixeira, M.J. Rosa, M. Nystrom, The role of membrane charge on nanofiltration performance, J. Membr. Sci. 265 (2005) 160–166.
[3] P.W. Morgan, Condensation Polymers: By Interfacial and Solution Methods, 19, Interscience, New York, NY, 1965.
[4] W. Xie, G.M. Geise, B.D. Freeman, H.-S. Lee, G. Byun, J.E. McGrath, Polyamide interfacial composite membranes prepared from m-phenylene diamine, trimesoyl chloride and a new disulfonated diamine, J. Membr. Sci. 403–404 (2012) 152–161.
[5] W.C. Chao, Y.-H. Huang, W.-S. Hung, Q. An, C.-C. Hu, K.-R. Lee, J.-Y. Lai, Effect of the surface property of poly(tetrafluoroethylene) support on the mechanism of polyamide active layer formation by interfacial polymerization, Soft Matter 8 (2012) 8998–9004.
[6] J. Lee, A. Hill, S. Kentish, Formation of a thick aromatic polyamide membrane by interfacial polymerisation, Sep. Purif. Technol. 104 (2013) 276–283.
[7] L. Lianchao, W. Baoguo, T. Huimin, C. Tianlu, X. Jiping, A novel nanofiltration membrane prepared with PAMAM and TMC by *in situ* interfacial polymerization on PEK-C ultrafiltration membrane, J. Membr. Sci. 269 (2006) 84–93.
[8] S. Veríssimo, K.V. Peinemann, J. Bordado, Influence of the diamine structure on the nanofiltration performance, surface morphology and surface charge of the composite polyamide membranes, J. Membr. Sci. 279 (2006) 266–275.

[9] H. Susanto, H. Arafat, E.M.L. Janssen, M. Ulbricht, Ultrafiltration of polysaccharide–protein mixtures: Elucidation of fouling mechanisms and fouling control by membrane surface modification, Sep. Purif. Technol. 63 (2008) 558–565.
[10] E.S. Kim, Y.J. Kim, Q. Yu, B. Deng, Preparation and characterization of polyamide thin-film composite (TFC) membranes on plasma-modified polyvinylidene fluoride (PVDF), J. Membr. Sci. 344 (2009) 71–81.
[11] S. Bequet, T. Abenoza, P. Aptel, J.M. Espenan, J.C. Remigy, A. Ricard, New composite membrane for water softening, Desalination 131 (2000) 299–305.
[12] M.N.A. Seman, M. Khayet, N. Hilal, Comparison of two different UV-grafted nanofiltration membranes prepared for reduction of humic acid fouling using acrylic acid and N-vinylpyrrolidone, Desalination 287 (2012) 19–29.
[13] B. Kaeselev, J. Pieracci, G. Belfort, Photoinduced grafting of ultrafiltration membranes: Comparison of poly (ether sulfone) and poly(sulfone), J. Membr. Sci. 194 (2001) 245–261.
[14] H. Deng, Y. Xu, Q. Chen, X. Wei, B. Zhu, High flux positively charged nanofiltration membranes prepared by UV-initiated graft polymerization of methacrylatoethyl trimethyl ammonium chloride (DMC) onto polysulfone membranes, J. Membr. Sci. 366 (2011) 363–372.
[15] T.A. Sergeyeva, H. Matuschewski, S.A. Piletsky, J. Bendig, U. Schedler, M. Ulbricht, Molecularly imprinted polymer membranes for substance-selective solid-phase extraction from water by surface photo-grafting polymerization, J. Chromatogr. A 907 (2001) 89–99.
[16] S. Luan, J. Zhao, H. Yang, H. Shi, J. Jin, X. Li, J. Liu, J. Wang, J. Yin, P. Stagnaro, Surface modification of poly (styrene-b-(ethylene-co-butylene)-b-styrene) elastomer via UV-induced graft polymerization of N-vinyl pyrrolidone, Colloids Surf., B: Biointerfaces 93 (2012) 127–134.
[17] S. Bequet, T. Abenoza, P. Aptel, J.M. Espenan, J.C. Remigy, A. Ricard, New composite membrane for water softening, Desalination 131 (2000) 299–305.
[18] D. He, H. Susanto, M. Ulbricht, Photo-irradiation for preparation, modification and stimulation of polymeric membranes, Prog. Polym. Sci. 34 (2009) 62–98.
[19] N. Hilal, M. Khayet, C.J. Wright, Membrane Modification, CRC Press, (2012) 235–237.
[20] M.A. Faruqi, H. Estrada, C. Gonzalez-Liendo, J.O. Sai, FRP Reinforced Concrete Exposed to Elevated Temperatures, Springer, 2012, pp. 113–122.
[21] V.S. Ivanov, Radiation-chemical transformations of polymers, in: New Concepts in Polymer Science: Radiation Chemistry of Polymers, C.R.H.I. de Jonge, (Ed.), Utrecht, The Netherlands, 1992, (Chapter 3).
[22] R.L. Clough, S.W. Shalaby, Radiation Effects on Polymers, ACS Publications, 1991.
[23] Y.T. Chung, L.Y. Ng, A.W. Mohammad, Sulfonated-polysulfone membrane surface modification by employing methacrylic acid through UV-grafting: Optimization through response surface methodology approach, J. Ind. Eng. Chem. 20 (2014) 1549–1557.
[24] Y. Mansourpanah, E. Momeni Habili, Preparation and modification of thin film PA membranes with improved antifouling property using acrylic acid and UV irradiation, J. Membr. Sci. 430 (2013) 158–166.
[25] C.L. Lai, Y.-J. Fu, J.-T. Chen, Q.-F. An, K.-S. Liao, Sh.-Ch Fang, Ch.-Ch. Hu, K.-R. Lee, Pervaporation separation of ethanol/water mixture by UV/O_3-modified PDMS membranes, Sep. Purif. Technol. 100 (2012) 15–21.
[26] G. Xueli, W. Haizeng, W. Jian, H. Xing, G. Congjie, Surface-modified PSf UF membrane by UV-assisted graft polymerization of capsaicin derivative moiety for fouling and bacterial resistance, J. Membr. Sci. 445 (2013) 146–155.
[27] A. Rahimpour, UV photo-grafting of hydrophilic monomers onto the surface of nano-porous PES membranes for improving surface properties, Desalination 265 (2011) 93–101.
[28] C. Qiu, Q.T.N.L. Zhang, Z. Ping, Nanofiltration membrane preparation by photomodification of cardo polyetherketone ultrafiltration membrane, Sep. Purif. Technol. 51 (2006) 325–331.
[29] A. Ahmad, B. Ooi, Properties–performance of thin film composites membrane: study on trimesoyl chloride content and polymerization time, J. Membr. Sci. 255 (2005) 67–77.
[30] K.L. Mittal, Contact Angle, Wettability and Adhesion, CRC Press, 2006.
[31] M. Bazel, The Effect of Solution Viscosity on the Flux and Rejection of Polyamide Membranes, Ben Gurion University, 2011.
[32] Y.-Q. Wang, Y.-L. Su, X.-L. Ma, Q. Sun, Z.-Y. Jiang, Pluronic polymers and polyethersulfone blend membranes with improved fouling-resistant ability and ultrafiltration performance, J. Membr. Sci. 283 (2006) 440–447.
[33] Y. Song, P. Sun, L.L. Henry, B. Sun, Mechanisms of structure and performance controlled thin film composite membrane formation via interfacial polymerization process, J. Membr. Sci. 251 (2005) 67–79.
[34] M.N. Abu Seman, M. Khayet, Z.I. Bin Ali, N. Hilal, Reduction of nanofiltration membrane fouling by UV-initiated graft polymerization technique, J. Membr. Sci. 355 (2010) 133–141.
[35] M. Ulbricht, Advanced functional polymer membranes, Polymer 47 (2006) 2217–2262.